(Received 10 March 2025, Accepted 9 June 2025, Scheduled 11 July 2025)

A Fabric-Based Double Rectangular Complementary Split Ring Resonator for Wideband Applications

Intan Shafinaz Abd. Razak[1], Zahriladha Zakaria[1,*], Ahmed Jamal Abdullah Al-Gburi[1], Maizatul Alice Meor Said[1], Ariffuddin Joret[2], Syah Alam[3], and Merih Palandoken[4]

[1] *Center for Telecommunication Research and Innovation (CeTRI), Fakulti Teknologi dan Kejuruteraan Elektronik dan Komputer (FTKEK), Universiti Teknikal Malaysia Melaka (UTeM), Malaysia*
[2] *Internet of Things Focus Group, Universiti Tun Hussein Onn Malaysia, (UTHM), Johor, Malaysia*
[3] *Department of Electrical Engineering, Universitas Trisakti, Indonesia*
[4] *Department of Electrical and Electronics Engineering, İzmir Kâtip Çelebi Üniversitesi, İzmir, Turkey*

ABSTRACT: This paper introduces a novel wideband antenna composed of fabric materials suitable for wearable and flexible applications and a straightforward single-unit Metamaterial (MTM). The antenna design employs ShieldIT Super as the conductive fabric and felt as the dielectric substrate, creating a lightweight and adaptable solution with dimensions of 58 mm × 34 mm × 2 mm. Operating over a frequency range of 1.88 to 6.88 GHz, the proposed antenna achieves a peak gain of 4.72 dBi and a radiation efficiency of 94%. The antenna has a wide measured bandwidth from 1.2 to 3.5 GHz (97%) and 4.0 to 5.9 GHz (38%), with an average measured gain of 3 dBi in the lower band and 4.6 dBi in the upper band. The MTM-inspired design features a double rectangular complementary split-ring resonator at the center of the radiating patch, which enhances bandwidth. The MTM structure exhibits Epsilon-Near-Zero (ENZ) and Mu-Negative (MNG) properties. This novel design illustrates significant advancements in wideband antenna performance and is suitable for wearable fabric-based S band, C band, 5G, Wireless Body Area Network (WBAN), and microwave imaging applications.

1. INTRODUCTION

Metamaterials (MTMs), engineered with unique electromagnetic properties not found in natural materials, have revolutionized various fields, including satellite communication, radar surveillance, medical devices, electronics, and agriculture. These advanced materials are also widely utilized in telemetry, vehicles, and wireless communication systems [1–3]. MTMs have significantly influenced antenna technology, enabling enhanced performance, compact designs, and novel functionalities for modern communication and sensing applications. In particular, these antennas use engineered materials to manipulate electromagnetic waves, improving bandwidth [4–9], gain [10–12], and directivity [13–18]. In addition, MTMs in antenna design can improve electromagnetic performance, especially in wearable and flexible communication devices, by integrating a reconfigurable approach and advanced material. This combination could enhance electrical conductivity, strength, versatility, and flexibility [19–21].

Enhancing antenna performance requires the complex design of MTM to obtain negative permittivity, permeability, and reflection index to ensure the manipulation of the wave contributes to the antenna systems [1, 2, 18, 19]. The complex design of a rigid substrate for MTM, as detailed in references [22] and [23], has led to the discovery of multiple resonances in the transmission coefficient. This design proves advantageous for applications within specific bandwidth ranges.

The growing demand for wearable electronics and seamless textile communication systems has fueled the significant development of fabric-based antennas [24]. Flexible, lightweight, body-conforming antennas are key to health monitoring, smart clothing, and on-body communication systems [25–27]. However, the design of compact, mechanically robust, wideband fabric antennas presents ongoing challenges. Wearable textile antennas have emerged as a significant area of research in recent studies, owing to their innovative designs that incorporate either thoroughly fabric materials or a combination of textiles. This contrasts with traditional rigid and stiff antenna structures, highlighting the potential for increased flexibility and comfort in various applications [5, 15, 16, 25–32].

Meanwhile, fabricating fabric-based MTMs will cause difficulty in their design fabrication and manufacturing costs. Utilizing an MTM unit cell array structure with an Epsilon-Negative (ENG) property and a Near-Zero Refractive Index (NZRI), the authors of [5] exhibit a textile ultra-wideband planar monopole antenna with a notably low gain at a lower frequency. The alternative fabric-based MTM is referenced in [16]. The MTM was positioned on the radiating patch's reverse side to improve directivity. Additionally, the design necessitates an active component, such as a varactor diode, to improve the reflection coefficient at lower frequencies.

The study presented in [15] proposed a complete fabric antenna constructed using 25 layers of polyester fabric to attain a thickness of 4 mm, demonstrating a notable gain of 9.43 dBi with eight units of an MTM structure. However, implementing

* Corresponding author: Zahriladha Zakaria (zahriladha@utem.edu.my).

multiple fabric layers increases fabrication complexity, possibly limiting its practicality for real-world applications. Similarly, the single-unit cell MTM patch antenna introduced in [31] employed jeans as the substrate material, achieving effective narrow dual-band operation. Despite its promising performance, the design suffers from significant drawbacks due to the material's susceptibility to crumpling, which can cause frequency shifts and compromise its consistency in wearable environments. The compact metasurface antenna by [32] can achieve stable performance. However, the design used a complex structure by inserting copper wire into the substrate.

In this study, the proposed antenna design contributes significant advancement by combining simplicity, wide operational bandwidth, and fully fabric-based construction within a compact footprint. The antenna employs a straightforward layout to utilize a single-layer textile substrate. The design achieves multi-band performance while maintaining mechanical flexibility and robustness under bending and on-body conditions.

The proposed antenna, inspired by MTMs and specifically designed for integration into textile applications, utilizes felt as a robust substrate. The inherent mechanical stability, flexibility, and resilience of felt make it suitable for wearable and flexible antenna applications. The proposed antenna enhances bandwidth by integrating a double rectangular Complementary Split Ring Resonator (CSRR). Incorporating a single unit CSRR enables effective bandwidth control by introducing multifrequency behavior. The CSRR and the gap between the rings can lead to bandwidth enhancement. The proposed antenna design is meticulously analyzed through simulations and measurements. It demonstrates its potential as a wideband, promising performance solution for wearable and fabric-based communications systems for many applications, including medical wireless devices.

2. ANTENNA DESIGN AND ANALYSIS

Figure 1 illustrates the design evolution of the antenna. The substrate type is felt, characterized as a fabric-based material with a thickness of 2 mm, a dielectric loss tangent of 0.02, and a relative permittivity of 1.39. The substrate material properties were obtained using coaxial probe method with an Agilent

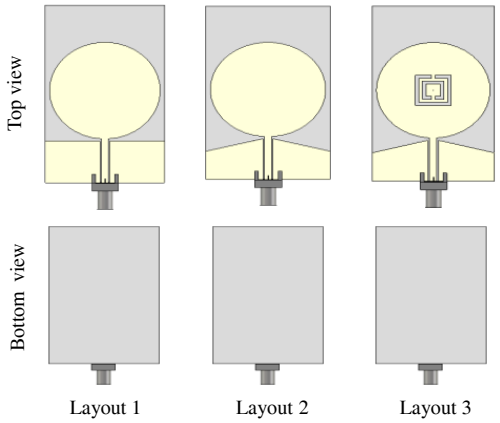

FIGURE 1. The evolution of the antenna design shows the top and bottom views.

Technologies N5242A Vector Network Analyzer (VNA). A Co-Planar Waveguide (CPW) antenna is constructed from conductive fabric material, specifically ShieldIT Super, which has a thickness of 0.17 mm and a conductivity of 1.18×10^5 S/m. The design initiates with a CPW-fed circular patch antenna (Layout 1), which produces dual bands. A trapezoidal ground plane (Layout 2) is implemented in the subsequent stages to achieve an extended bandwidth. Introducing the double rectangular CSRRs positioned at the center of the circular patch (Layout 3) improves the reflection coefficient across the entire bandwidth.

The CPW antenna was engineered to achieve the required bandwidth by implementing a modified half-trapezium ground plane. The advantages of CPW are that one side-radiator and ground plane are on a single side, and it is easy to integrate with another application [33]. Figure 2 illustrates the geometry and dimensions of the CPW antenna. The CPW antenna formula is derived from calculations based on [34]. Applying Equation (1) allows for predicting its lower resonant frequency.

$$fr = \frac{14.4}{l1 + l2 + g1 + \frac{A1}{2\pi l1\sqrt{(\varepsilon r+1)/2}} + \frac{A2}{2\pi l2\sqrt{(\varepsilon r+1)/2}}}. \quad (1)$$

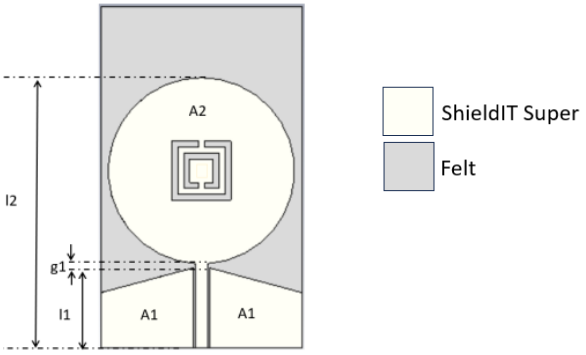

FIGURE 2. The CPW antenna is based on a modified circle-shaped patch and trapezoid ground plane.

The dimensions of the ground plane and radiating patch are denoted as $l1$ and $l2$, respectively. Parameter $g1$ represents the distance between the patch radiator and ground plane, while $A1$ and $A2$ refer to the areas of the ground plane and radiating patch, respectively. All measurements for $l1$, $l2$, $g1$, $A1$, and $A2$ are expressed in centimetres. εr represents the dielectric constant of the substrate material. The antenna has a circle diameter of 36 mm. Additional geometrical parameters are detailed in Figure 3 and Table 1.

Fundamentally, the proposed double rectangular CSRR design is initiated by choosing 6 GHz as the resonance frequency and calculating the maximum length and width of the design as approximately 12 mm ($\lambda/4$). Consequently, the double rectangular CSRR dimensions are defined using Computer Simulation Technology (CST) Microwave Studio to achieve a wide bandwidth. The proposed MTM-inspired antenna was simulated using the configuration described in [35], displayed in Figure 4(a). Figure 4(b) illustrates that the transmission coefficients operate over the the frequency range of 4.8 GHz to 7.6 GHz. The reflection and transmission coefficient values are

TABLE 1. Geometric parameters of the proposed antenna (mm).

Parameters	**Ws**	**Ls**	**Ga**	**Gb**	**Gc**	**Wf**	**Lf**	
Values (mm)	34	58	9.42	13.6	15.6	2	14.33	
Parameters	**a**	**b**	**c**	**d**	**e**	**f**	**g**	**h**
Values (mm)	10	8	6	4	4.5	3.5	2.5	1.5

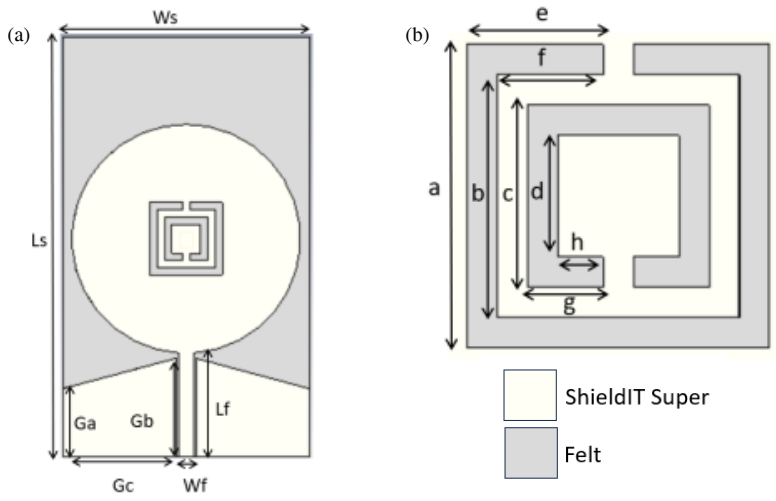

FIGURE 3. (a) Patch, feedline, and ground dimension and (b) the double rectangular CSRR dimension of the CPW antenna.

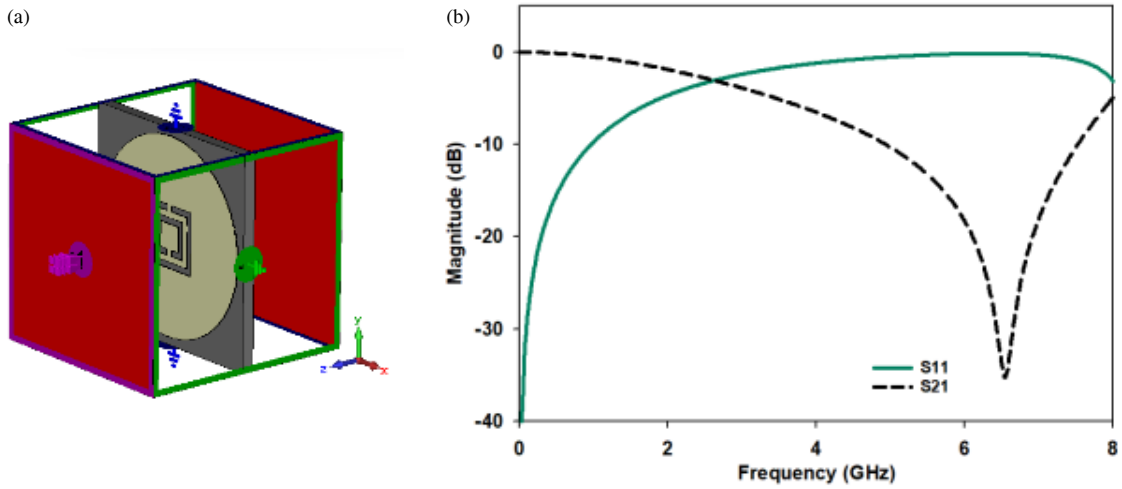

FIGURE 4. (a) Simulation boundaries setup, (b) reflection coefficient (S_{11}), and transmission coefficient (S_{21}).

applied in the Nicolson Ross Weir approach to extract the MTM properties such as permittivity, permeability, and refractive index [36].

The target MTM performance is between 3 and 6 GHz to enhance bandwidth. Figure 5(a) illustrates the observation of Epsilon-Near-Zero (ENZ) properties at 2.4 to 5.5 GHz, whereas Figure 5(b) demonstrates the observation of negative permeability, MNG in the range of 4.2 GHz to 7.9 GHz. The structural characteristics of the suggested design demonstrated MTM-like behavior at designated frequencies. Figure 5(c) depicts the negative reflective index at 2.8 to 5.5 GHz. Meanwhile, the negative reading is extended to 6.2 to 8.7 GHz, and the frequency range 5.5 to 6.2 GHz exhibits NZRI. Subsequently, after obtaining the negative quantity of permittivity and permeability, the dimension is conveyed to the CPW antenna, as pictured in Figure 3. The examination of the proposed antenna is conducted in the subsequent subsections.

An equivalent quasi-static LC circuit can describe the CSRR resonance, and its resonance frequency (f) is defined by Equation (2) [37]. L is the inductance of the rectangular rings, and

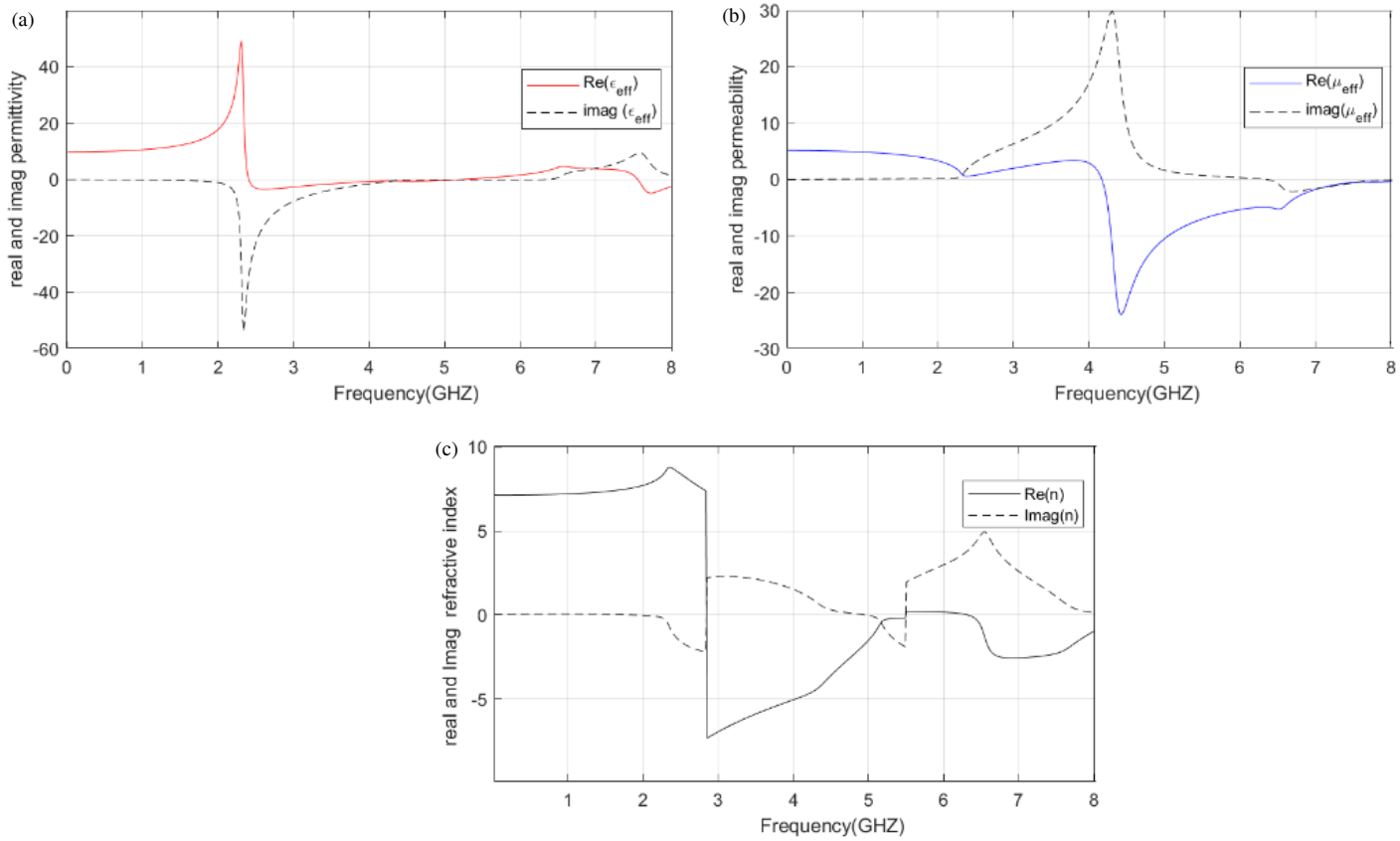

FIGURE 5. Double CSRRs (a) permittivity, (b) permeability, and (c) refractive index.

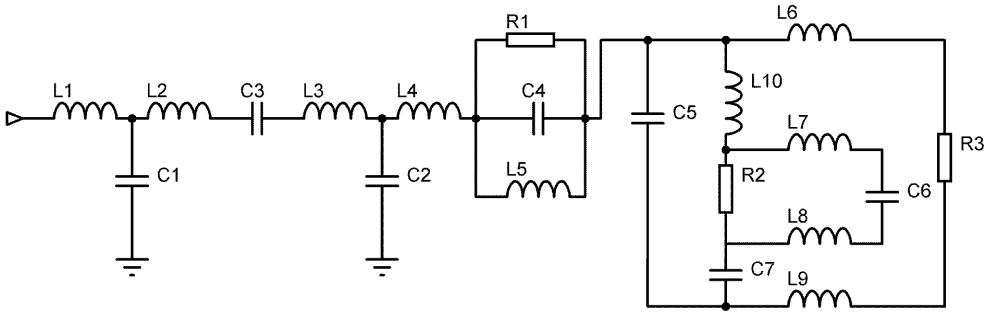

FIGURE 6. Equivalent circuit representation of proposed antenna.

C is the capacitance between them:

$$f = \frac{1}{2\pi(LC)^{0.5}}. \tag{2}$$

Figure 6 illustrates the equivalent circuit simulation with CPW, a circular patch, and CSRRs represented as lumped components. C_5 and L_6 represent the outer ring, while C_6 and L_7 represent the inner ring. C_7 denotes capacitive connection, while L_8 and L_9 indicate inductive coupling [38]. The equivalent circuit is constructed using Cadence AWR Microwave Office software, and the values of each lumped component are adjusted to obtain a resonance frequency that aligns with the simulation results. The value acquired are $L_1 = 1.51\,\text{nH}$, $L_2 = 3.86\,\text{nH}$, $L_3 = 1.04\,\text{nH}$, $L_4 = 1.89\,\text{nH}$, $L_5 = 1.13\,\text{nH}$, $L_6 = 0.42\,\text{nH}$, $L_7 = 0.98\,\text{nH}$, $L_8 = 1.99\,\text{nH}$, $L_9 = 1.80\,\text{nH}$, $L_{10} = 43.08\,\text{nH}$, $C_1 = 0.66\,\text{pF}$, $C_2 = 0.58\,\text{pF}$, $C_3 = 0.84\,\text{pF}$, $C_4 = 1.58\,\text{v}$, $C_5 = 10.78\,\text{pF}$, $C_6 = 1.12\,\text{pF}$, $C_7 = 21.60\,\text{pF}$, $\text{R}_1 = 34.5\,\Omega$, $R_2 = 32.16\,\Omega$, and $R_3 = 63.08\,\Omega$. Figure 7 illustrates the comparison of the reflection coefficients between the equivalent circuit model of the proposed antenna designed using Cadence AWR and the simulation in CST. The calculated value indicates that the outer ring frequency is 2.36 GHz, while the inner ring is 4.80 GHz.

3. RESULT AND DISCUSSION

The analysis of surface current distribution provides insight into the resonant behaviour and bandwidth performance of the proposed antenna design. The surface current distribution on Lay-

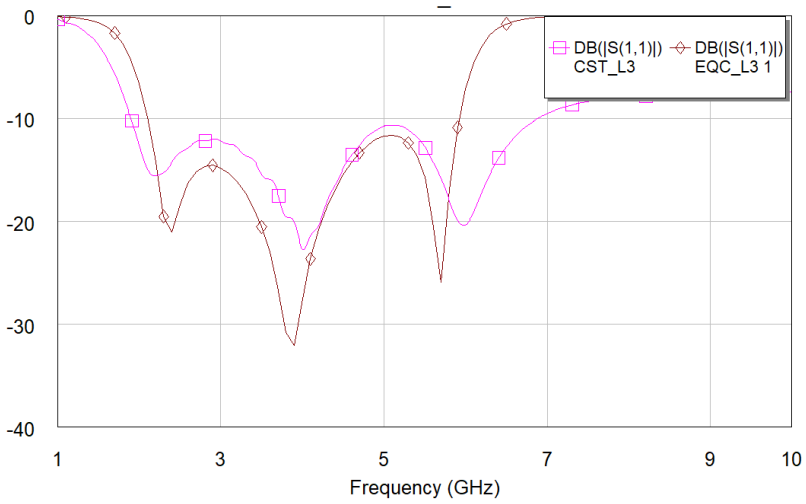

FIGURE 7. Comparison of the reflection coefficient of the equivalent circuit (Cadence AWR) and antenna simulation (CST).

TABLE 2. Comparison of antenna parameters based on their layout's evolution.

Characteristics	Layout 1	Layout 2	Layout 3
Bandwidth (GHz)	2.09–4.23 & 5.55–8.33	1.91–4.84 & 5.23–6.85	1.88–6.88
Gain range (dBi)	1.21–4.01 & 1.84–4.71	1.10–3.33 & 3.19–4.85	1.04–4.72
Radiation Efficiency (%)	85–93	85–93	88–94

outs 2 and 3 at 2.45, 3, 3.5, 4,5, 5.8, 6, and 6.5 GHz supports the evidence of improvement in broad bandwidth enhancement. Figures 8(a) to (p) illustrate the surface current corresponding to a simulation phase angle configuration of 0°. The maximum current is set up to 10 A/m to acquire a fair comparison of current density based on the color scale to illustrate the difference between Layout 2 and Layout 3 surface currents. The geometry of the slot influences the surface current distribution both in the presence and absence of double rectangular CSRRs positioned at the center of the circular patch. The design of Layout 3 incorporates a slot that effectively reduces the reflection coefficient within the frequency range of 4.8 GHz to 5.2 GHz, thereby enhancing the antenna's bandwidth compared to Layout 2. The analysis is derived from comparing the current density at the radiating patch. Based on previous calculations on lumped elements, the outer ring operates at lower frequencies and the inner ring at higher frequencies. As proved, the outer slot reacts at lower frequencies (3, 3.5, and 4 GHz), and the inner slot responds at a higher frequency (5.8 and 6 GHz).

The MTM element with a CSRR modifies the current flow, enhancing bandwidth. Referring to the MTM analysis in Figures 5(a) and (b), the negative permittivity and permeability are obtained at lower and higher frequency bands, respectively. Thus, the structure exhibits a single negative behaviour at two regions of the frequency band. The permittivity ranges from 2.4 to 4.1 GHz (outer ring). Meanwhile, permeability operates at 4.2 to 7.9 GHz (inner ring).

The approach demonstrates an improvement in bandwidth for Layout 1 (dual bands with 67% and 40%) to Layout 2 (dual bands with 87% and 27%) for lower and upper band frequencies. As evidenced in Figures 9(a) and (b), implementing double rectangular CSRRs, MTM-inspired antenna improves the reflection coefficient and Voltage Standing Wave Ratio (VSWR) of the antenna. The graph displayed in Figure 9(c) depicts the proposed antenna's gain. The efficiency of all the designs illustrated in Figure 9(d) highlights the overall radiation performance up to 85% over the operating frequencies. The summary of the antenna design is listed in Table 2.

The measurement using VNA from Agilent Technologies model N5242A for the S-parameter is presented in Figure 10(b). Figures 10(e) and (e) illustrate the normalized measured and simulated gains and radiation efficiencies over operating frequencies. The maximum measured gain and radiation efficiency are 5 dBi and 83%, respectively. Even though the reflection coefficient has slight alterations at frequencies and changes in resonance frequencies, there are still acceptable outputs in Wireless Body Area Network (WBAN) applications. More importantly, the impedance bandwidth ($S_{11} \leq -10$ dB), 1.2–3.5 GHz (97%), and 4.0–5.9 GHz (38%) cover the wideband frequency region. To investigate the different simulation and measurement results, Figure 11 illustrates factors that may contribute to the differences. Figures 11(a) and (b) depict the effect of permittivity and loss tangent of the substrate material. The findings demonstrate that minor fluctuations in these param-

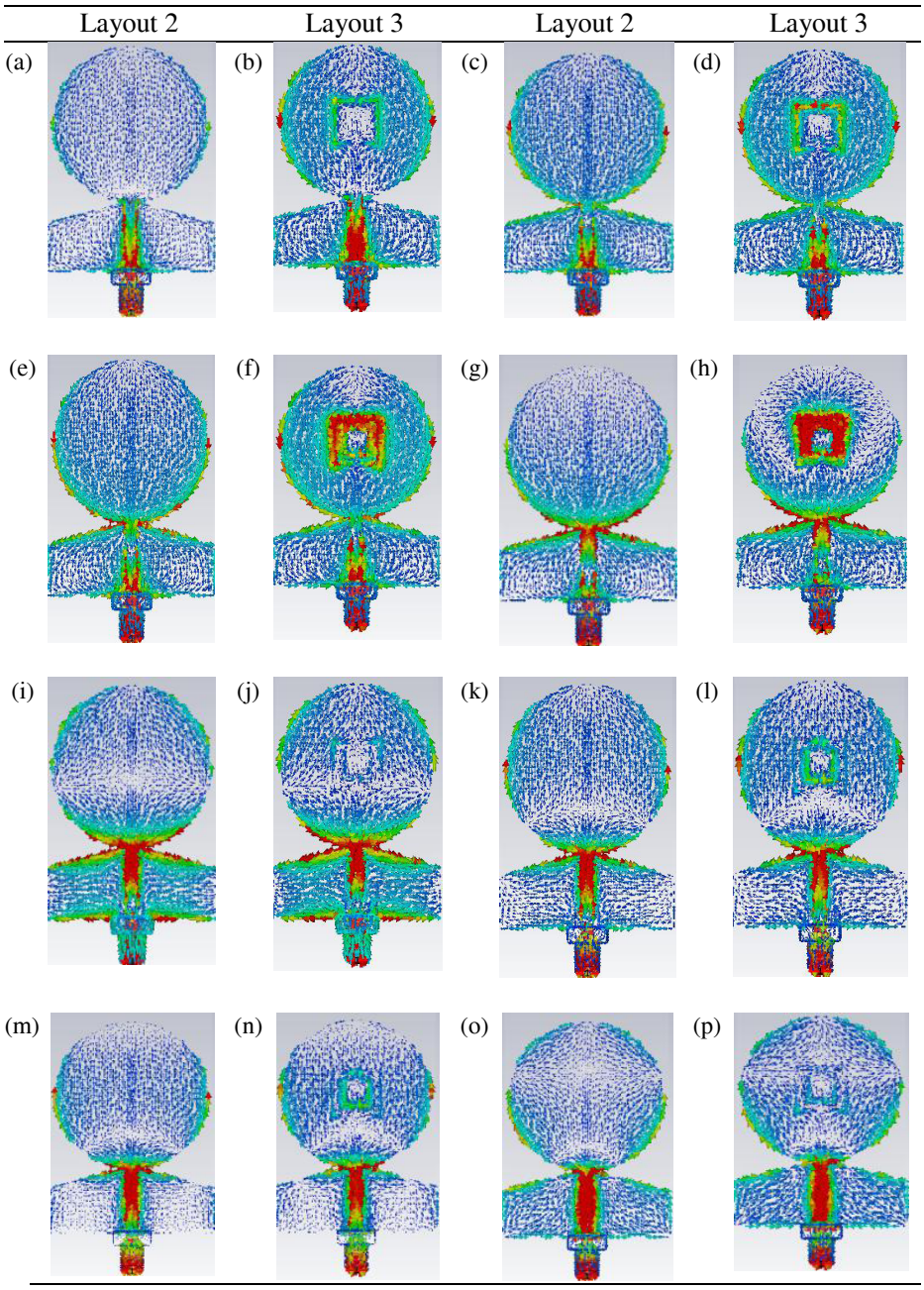

FIGURE 8. The current distribution comparison between Layouts 2 and 3 of the CPW antenna. (a) 2.45 GHz, (b) 2.45 GHz, (c) 3 GHz, (d) 3 GHz, (e) 3.5 GHz, (f) 3.5 GHz, (g) 4 GHz, (h) 4 GHz, (i) 5 GHz, (j) 5 GHz, (k) 5.8 GHz, (l) 5.8 GHz, (m) 6 GHz, (n) 6 GHz, (o) 6.5 GHz, (p) 6.5 GHz.

eters have a negligible impact on the resonant frequency and return loss. Variations in substrate thickness and ring gap of CSRR have a minimal effect on antenna performance, as depicted in Figures 11(e) and (d), respectively. Due to the manual cutting involved in this study, the dimensions of the CSRRs and the spacing between the feedline and ground are critical factors. The fabrication imperfections replicate potential discrepancies during measurement, as displayed in Figures 11(c) and (f). The findings indicate that even a slight discrepancy and misalignment between the feedline and CSRR dimensions can lead to detuning or alterations in the reflection coefficient. Through these supplementary simulations, practical fabrication factors have been demonstrated. Meanwhile, the observed differences between measurement and simulation may occur from fabrication tolerances. This is mainly due to a 50 Ω impedance mismatch across various frequency bands [39], and due to the fabric nature and thickness the bandwidth tends to shift to lower frequencies [40].

Figure 12 illustrates the fabricated antenna's simulated and measured radiation patterns at three key operating frequencies: 2.45 GHz, 3.5 GHz, and 5.8 GHz. These frequencies correspond to the targeted multi-band operation of the antenna, de-

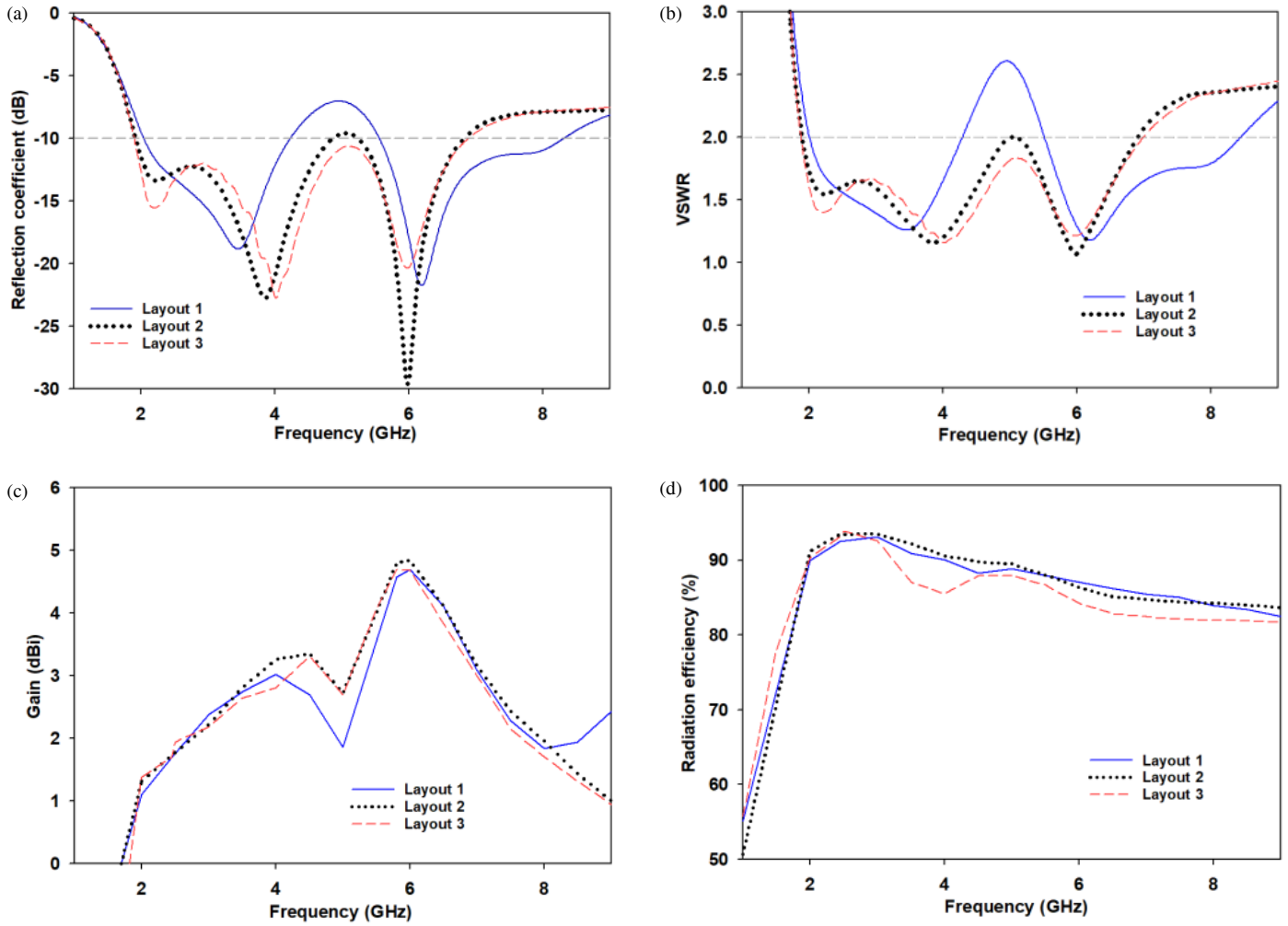

FIGURE 9. Simulation of proposed antenna evolution comparison of (a) reflection coefficient, (b) VSWR, (c) realized gain, and (d) radiation efficiency.

signed for various wireless communication applications. The top row of the figure presents the simulated 3D radiation patterns, while the bottom row displays the 2D polar plots in electric (red lines) and magnetic (green line) planes. It can be observed that the antenna exhibits predominantly omnidirectional or bidirectional characteristics across the operating bands, which is favourable for broad coverage in practical deployment scenarios.

The primary concern for wearable antennas, when being used near or in contact with human tissues, is the body's potential absorption of electromagnetic radiation. Specific Absorption Rate (SAR) quantifies the rate of radio frequency energy absorption by biological tissues. Regulatory standards, such as IEEE C95.1-2005, specify a maximum SAR limit of 2 W/kg for planar configurations positioned above a human [32]. This study utilized a head model due to its significance as a critical and highly sensitive part of the human body. Figure 13 illustrates that the peak SAR values are measured at an input power of an accepted power level of 25 mW [41]. The corresponding SAR values were 0.127 W/kg at 2.45 GHz, 0.0774 W/kg at 3.5 GHz, and 0.124 W/kg at 5.8 GHz at a 5 mm gap from the human head model.

Finally, Figures 14 and 15 evaluate the proposed fabric-based antenna's mechanical flexibility and on-body performance by analyzing its reflection coefficient under different bending conditions and in proximity to the human body. In Figure 14, the proposed antenna maintains wideband operation even under bending, achieving 108% and 112% bandwidths for curvature diameters of 40 mm and 60 mm, respectively. The results reveal that the antenna maintains its multi-band resonance characteristics even under significant mechanical deformation. Nevertheless, the stable behaviour under bending confirms the antenna's robustness and suitability for flexible or wearable applications.

Figure 15 compares the antenna's performance on the shoulder and wrist in free space. Dielectric loading and absorption in human tissue affect antenna impedance and resonance. Despite these impacts, the antenna maintains resonance in the target bands with relatively small frequency and return loss changes. High-permittivity biological tissues around the antenna change its near-field environment, causing these alterations. The re-

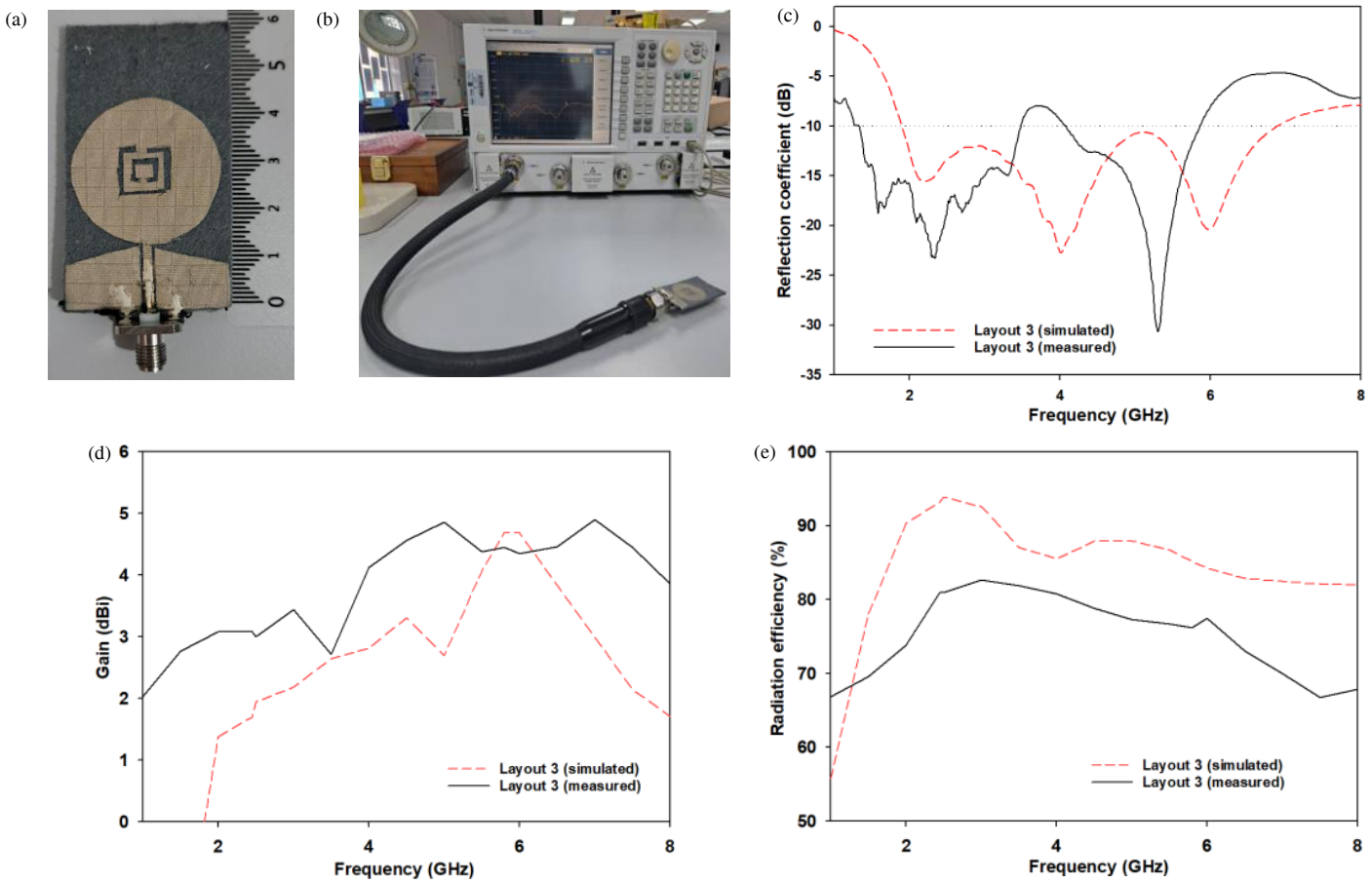

FIGURE 10. The proposed antenna (a) has a front view of the fabricated antenna, and (b) the measurement is set up with VNA. (c) reflection coefficient, (c) realized gain, and (d) radiation efficiency of simulated and measured proposed antenna.

TABLE 3. Comparison of the proposed antenna with other similar fabric-based MTM-inspired antennas.

Researcher	Bandwidth (GHz & (%))	Peak Gain (dBi)	Peak Efficiency (%)	Number of a unit cell	Material	Mechanical flexibility	Electrical dimension ($\lambda_0 \times \lambda_0 \times \lambda_0$)	Fabrication complexity
[5]	2.55–15 (141)	4.84	87	8	Felt	Yes	$0.28 \times 0.25 \times 0.02$	Medium
[15]	4.2–4.8 (13)	9.43	94.5	8	Polyester	Yes	$0.70 \times 1.05 \times 0.05$	High
[16]	2.4–3.2 (28), 4–15 (115)	7.56	76	2	Felt	Yes	$0.64 \times 0.48 \times 0.04$	High
[31]	1.6–2.56 (46), 4.24–7 (49)	2 6	NR	1	Jeans	Yes	$0.32 \times 0.32 \times 0.01$	Low
[32]	2.25–2.5 (10) 5.21–6.45 (23)	−0.69 7.4	42	16	Felt	Yes	$0.36 \times 0.36 \times 0.04$	High
Proposed	1.88–6.88 (114)	4.72	94	1	Felt	Yes	$0.36 \times 0.21 \times 0.01$	Low

flection coefficient stays below −10 dB at crucial working frequencies, proving that the antenna may work in wearable applications. The results in both figures validate the antenna's mechanical and electromagnetic resilience, making it a promising candidate for integration into wearable and body-centric wireless communication systems.

Table 3 compares the proposed antenna with the previous fabric-based material MTM antennas, focusing on bandwidth, gain, radiation efficiency, dimension, the number of unit cells, material, and fabrication complexity. The proposed antenna demonstrates several advancements compared to the designs of previous researchers, particularly in terms of bandwidth, effi-

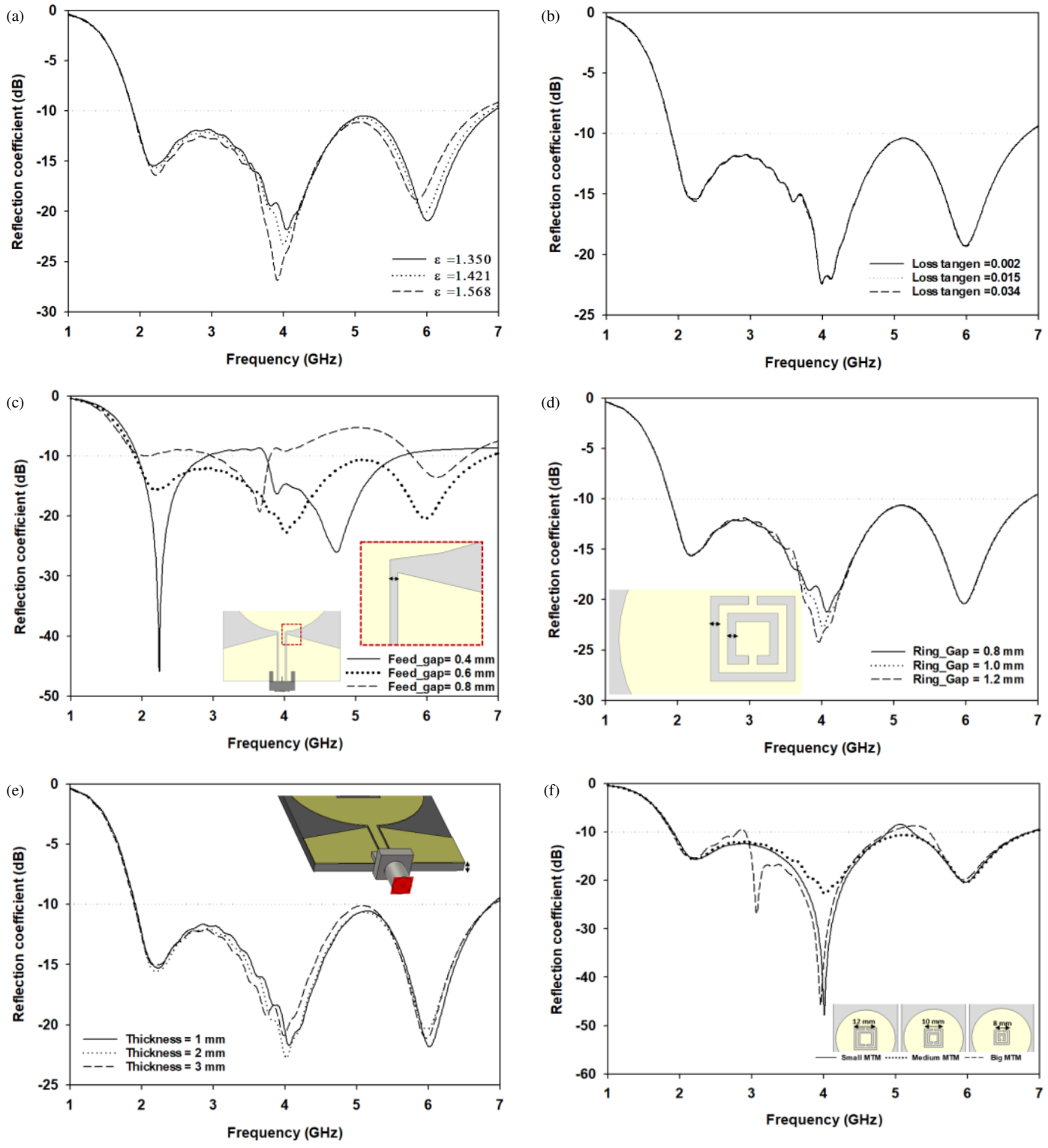

FIGURE 11. The parametric study of antenna design is based on (a) relative permittivity of the substrate, (b) loss tangent, (c) feedline gap with the ground of CPW, (d) ring gap of CSRR, (e) substrate thickness, and (f) size of CSRR.

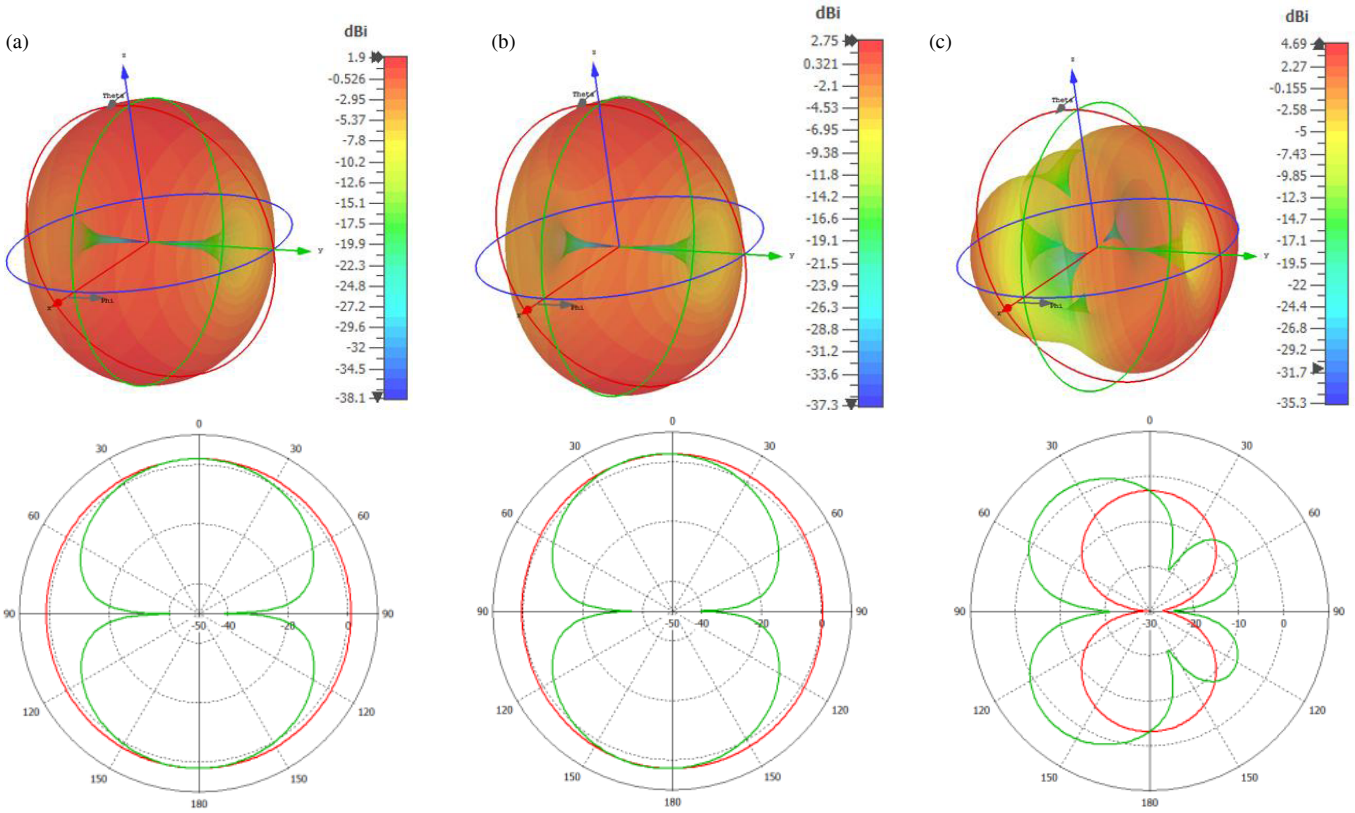

FIGURE 12. Simulated radiation pattern of proposed antenna at (a) 2.45, (b) 3.5 GHz, and (c) 5.8 GHz in 3D (top) and 2D (bottom).

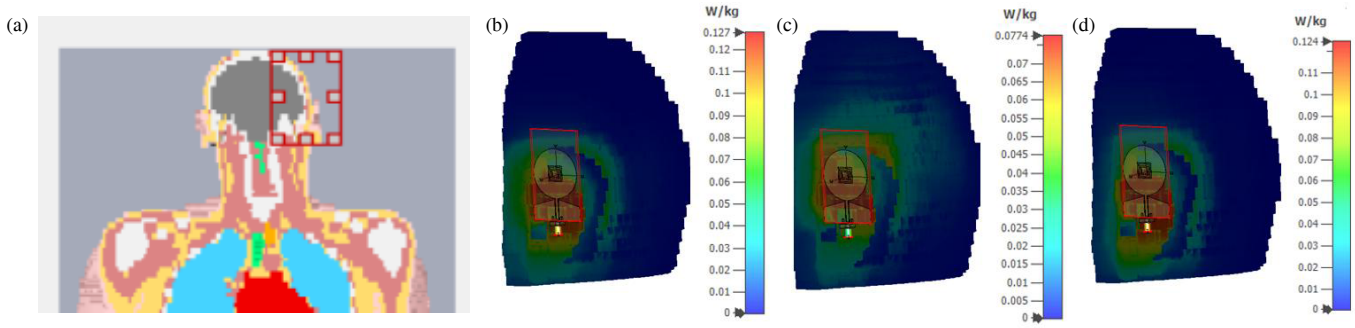

FIGURE 13. Simulated SAR of the antenna on (a) human head model at (b) 2.45, (c) 3.5 GHz, and (d) 5.8 GHz.

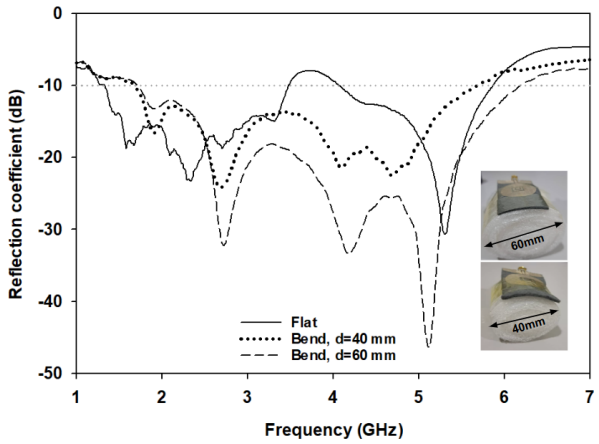

FIGURE 14. Measured bending analysis of the antenna.

ciency, and simplicity of design. Using a single unit cell in the proposed antenna reduces the complexity and manufacturing costs while maintaining appropriate performance. The proposed antenna achieves a competitive balance of wide bandwidth, high efficiency, and low fabrication complexity by utilizing fabric-based construction within a compact footprint. The antenna features a simple design that removes the necessity for active components, embedded wires, or multilayer stacking, thus reducing fabrication complexity and improving practical applicability. The design employs a single-layer textile substrate to achieve stable multi-band performance, ensuring mechanical flexibility and robustness during bending and on-body conditions.

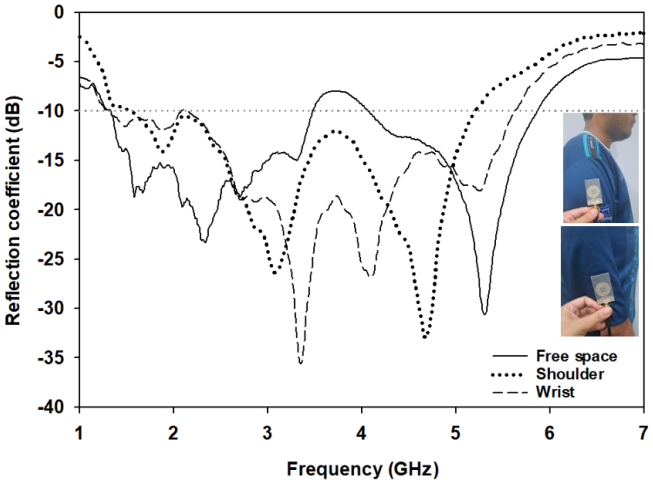

FIGURE 15. Measured performance on the human body.

4. CONCLUSION

This study has presented the design and experimental validation of an MTM-inspired antenna utilizing a fabric-based material for wideband applications. The proposed design achieved a wide operating bandwidth, acceptable gain, and compact structure, making it highly suitable for integrating modern wireless communication systems. A novel and straightforward approach was employed by incorporating double rectangular CSRRs at the center of a circular patch antenna, effectively enhancing the frequency response. This implementation leveraged ENZ properties at lower frequencies and MNG properties at higher frequencies, significantly improving the reflection coefficient across the bandwidth. The results demonstrate the antenna's potential for wearable communication devices and on-body electromagnetic medical diagnosis applications.

ACKNOWLEDGMENT

The authors gratefully acknowledge UTeM for funding support. This study was conducted during the author's study leave under the 2022 Federal Training (HLP) scholarship by MOHE.

REFERENCES

[1] Esmail, B. A. F., S. Koziel, and S. Szczepanski, "Overview of planar antenna loading metamaterials for gain performance enhancement: the two decades of progress," *IEEE Access*, Vol. 10, 27 381–27 403, 2022.

[2] Iqbal, K. and Q. U. Khan, "Review of metasurfaces through unit cell design and numerical extraction of parameters and their applications in antennas," *IEEE Access*, Vol. 10, 112 368–112 391, 2022.

[3] Abdullah, S., G. Xiao, and R. E. Amaya, "A review on the history and current literature of metamaterials and its applications to antennas & radio frequency identification (RFID) devices," *IEEE Journal of Radio Frequency Identification*, Vol. 5, No. 4, 427–445, 2021.

[4] Alibakhshikenari, M., B. S. Virdee, P. Shukla, N. O. Parchin, L. Azpilicueta, C. H. See, R. A. Abd-Alhameed, F. Falcone, I. Huynen, T. A. Denidni, and E. Limiti, "Metamaterial-inspired antenna array for application in microwave breast imaging systems for tumor detection," *IEEE Access*, Vol. 8, 174 667–174 678, 2020.

[5] Hossain, K., T. Sabapathy, M. Jusoh, M. A. Abdelghany, P. J. Soh, M. N. Osman, M. N. M. Yasin, H. A. Rahim, and S. S. Al-Bawri, "A negative index nonagonal CSRR metamaterial-based compact flexible planar monopole antenna for ultrawideband applications using viscose-wool felt," *Polymers*, Vol. 13, No. 16, 2819, 2021.

[6] Daniel, R. S., R. Pandeeswari, and S. Raghavan, "A compact metamaterial loaded monopole antenna with offset-fed microstrip line for wireless applications," *AEU — International Journal of Electronics and Communications*, Vol. 83, 88–94, 2018.

[7] Ahmed, S., Z. A. A. Hassain, H. A. Abdulnabi, and M. Al-Saadi, "Design and bandwidth enhancement of zeroth-order resonator antenna using metamaterial," *Telkomnika (Telecommunication Computing Electronics and Control)*, Vol. 20, No. 3, 494–500, 2022.

[8] Ennajih, A., J. Zbitou, M. Latrach, A. Errkik, L. Abdellaoui, and A. Tajmouati, "A novel design of a miniature metamaterial antenna for RFID reader applications," *Telkomnika (Telecommunication Computing Electronics and Control)*, Vol. 16, No. 1, 174–181, 2018.

[9] Ghanbari, L., A. Keshtkar, and S. Jarchi, "A novel metamaterial-inspired UWB and ISM multiband antenna for wireless communications: Design and characteristic mode analysis," *Progress In Electromagnetics Research C*, Vol. 136, 1–12, 2023.

[10] Abdelghany, M. A., M. F. A. Sree, A. Desai, and A. A. Ibrahim, "Gain improvement of a dual-band CPW monopole antenna for sub-6 GHz 5G applications using AMC structures," *Electronics*, Vol. 11, No. 14, 2211, 2022.

[11] Chaouche, Y. B., M. Nedil, I. B. Mabrouk, and O. M. Ramahi, "A wearable circularly polarized antenna backed by AMC reflector for WBAN communications," *IEEE Access*, Vol. 10, 12 838–12 852, 2022.

[12] Muhammad, H. A., Y. I. Abdulkarim, P. A. Abdoul, H. N. Awl, F. A. Teksen, F. O. Alkurt, M. Karaaslan, M. Bakır, and B. Appasani, "A highly flexible and low-profile metasurface antenna for wearable WBAN systems," *Optik*, Vol. 313, 171974, 2024.

[13] Islam, M. T., M. T. Islam, M. Samsuzzaman, H. Arshad, and H. Rmili, "Metamaterial loaded nine high gain vivaldi antennas array for microwave breast imaging application," *IEEE Access*, Vol. 8, 227 678–227 689, 2020.

[14] Al-Gburi, A. J. A., I. B. M. Ibrahim, M. Y. Zeain, and Z. Zakaria, "Compact size and high gain of CPW-fed UWB strawberry artistic shaped printed monopole antennas using FSS single layer reflector," *IEEE Access*, Vol. 8, 92 697–92 707, 2020.

[15] Çelenk, E. and N. T. Tokan, "All-textile on-body metasurface antenna," *Progress In Electromagnetics Research M*, Vol. 110, 119–131, 2022.

[16] Hossain, K., T. Sabapathy, M. Jusoh, S.-H. Lee, K. S. A. Rahman, and M. R. Kamarudin, "Negative index metamaterial-based frequency-reconfigurable textile CPW antenna for microwave imaging of breast cancer," *Sensors*, Vol. 22, No. 4, 1626, 2022.

[17] Moumen, I., M. Elhabchi, M. N. Srifi, and R. Touahni, "Metamaterial inspired circular antenna for Bluetooth band integration," *Telkomnika (Telecommunication Computing Electronics and Control)*, Vol. 22, No. 3, 510–518, 2024.

[18] Nayat-Ali, O., F. Z. Khoutar, M. Aznabet, O. E. Mrabet, and M. Khalladi, "A low-cost four circularly polarized antenna loaded with a complementary split ring resonator for beam steering applications," *Progress In Electromagnetics Research C*, Vol. 152, 13–18, 2025.

[19] Abdollahvand, M., E. Martinez-de Rioja, J. A. Encinar, K. Katoch, A. Ebrahimi, and S. Ghosh, "Reconfigurable FSS with a switchable passband for space applications in X and Ka bands," in *2022 16th European Conference on Antennas and Propagation (EuCAP)*, 1–4, Madrid, Spain, Mar. 2022.

[20] Abdollahvand, M., E. Martinez-de Rioja, J. A. Encinar, and K. Katoch, "Dual-band single-layer frequency selective surface for millimeter-Wave 5G applications," in *2023 17th European Conference on Antennas and Propagation (EuCAP)*, 1–3, Florence, Italy, Mar. 2023.

[21] Al-Gburi, A. J. A., M. M. Ismail, N. J. Mohammed, and T. A. H. Alghamdi, "SAR flexible antenna advancements: Highly conductive polymer-graphene oxide-silver nanocomposites," *Progress In Electromagnetics Research M*, Vol. 127, 23–30, 2024.

[22] Hossain, M. B., M. R. I. Faruque, A. S. Alshammari, and M. T. Islam, "Wide bandwidth enriched symmetric hexagonal split ring resonator based triple band negative permittivity metamaterial for satellite and Wi-Fi applications," *Results in Physics*, Vol. 37, 105511, 2022.

[23] Hussain, A., J. Dong, Y. I. Abdulkarim, R. Wu, F. F. Muhammadsharif, R. Shi, and M. M. R. Howlader, "A double negative (DNG) metamaterial based on parallel double-E square split resonators for multi-band applications: Simulation and experiment," *Results in Physics*, Vol. 46, 106302, 2023.

[24] Mahmood, S. N., A. J. Ishak, T. Saeidi, H. Alsariera, S. Alani, A. Ismail, and A. C. Soh, "Recent advances in wearable antenna technologies: A review," *Progress In Electromagnetics Research B*, Vol. 89, 1–27, 2020.

[25] Radi, N. H. M., M. M. Ismail, Z. Zakaria, J. A. Razak, and S. N. I. Abdullah, "Development and design of wearable textile antenna on various fabric substrate for unlicensed ultra-wideband applications," *Telkomnika (Telecommunication Computing Electronics and Control)*, Vol. 20, No. 6, 1181–1188, 2022.

[26] Muhammad, H. A., Y. I. Abdulkarim, P. A. Abdoul, and J. Dong, "Textile and metasurface integrated wide-band wearable antenna for wireless body area network applications," *AEU — International Journal of Electronics and Communications*, Vol. 169, 154759, 2023.

[27] Nurhayati, N., A. N. D. N. Fahmi, P. Puspitaningayu, O. Wiriawan, B. Raafi'u, F. A. Iskandarianto, A. J. A. Al-Gburi, A. Varshney, and S. Johari, "Wearable wideband textile coplanar vivaldi antenna for medical and IoT application," *Progress In Electromagnetics Research C*, Vol. 148, 145–156, 2024.

[28] Yalduz, H., T. E. Tabaru, V. T. Kilic, and M. Turkmen, "Design and analysis of low profile and low SAR full-textile UWB wearable antenna with metamaterial for WBAN applications," *AEU — International Journal of Electronics and Communications*, Vol. 126, 153465, 2020.

[29] Elsheakh, D. M., S. A. Alsherif, and A. R. Eldamak, "Textile monopole sensors for breast cancer detection," *Telecommunication Systems*, Vol. 82, No. 3, 363–379, 2023.

[30] Mahmood, S. N., A. J. Ishak, T. Saeidi, A. C. Soh, A. Jalal, M. A. Imran, and Q. H. Abbasi, "Full ground ultra-wideband wearable textile antenna for breast cancer and wireless body area network applications," *Micromachines*, Vol. 12, No. 3, 322, 2021.

[31] Roy, S. and U. Chakraborty, "Metamaterial based dual wideband wearable antenna for wireless applications," *Wireless Personal Communications*, Vol. 106, No. 3, 1117–1133, 2019.

[32] Zhang, K., P. J. Soh, and S. Yan, "Design of a compact dual-band textile antenna based on metasurface," *IEEE Transactions on Biomedical Circuits and Systems*, Vol. 16, No. 2, 211–221, Apr. 2022.

[33] Hussain, M., M. A. Sufian, M. S. Alzaidi, S. I. Naqvi, N. Hussain, D. H. Elkamchouchi, M. F. A. Sree, and S. Y. A. Fatah, "Bandwidth and gain enhancement of a CPW antenna using frequency selective surface for UWB applications," *Micromachines*, Vol. 14, No. 3, 591, 2023.

[34] Gupta, N., J. Saxena, K. S. Bhatia, and R. Kumar, "A compact CPW-fed planar stacked circle patch antenna for wideband applications," *Wireless Personal Communications*, Vol. 116, No. 4, 3247–3260, 2021.

[35] Hossen, M. S., A. Hoque, M. T. Islam, P. Kirawanich, M. H. Baharuddin, H. Alsaif, and M. S. Soliman, "DNG metamaterial-inspired slotted stub antenna with enhanced gain, efficiency and distributed current for early stage bone fracture detection applications," *IEEE Sensors Journal*, Vol. 24, No. 22, 37 932–37 946, 2024.

[36] Dawar, P., N. S. Raghava, and A. De, "UWB metamaterial-loaded antenna for C-band applications," *International Journal of Antennas and Propagation*, Vol. 2019, No. 1, 6087039, 2019.

[37] Milias, C., R. B. Andersen, P. I. Lazaridis, Z. D. Zaharis, B. Muhammad, J. T. B. Kristensen, A. Mihovska, and D. D. S. Hermansen, "Metamaterial-inspired antennas: A review of the state of the art and future design challenges," *IEEE Access*, Vol. 9, 89 846–89 865, 2021.

[38] Bahl, I. J., *Lumped Elements for RF and Microwave Circuits*, Artech House, 2022.

[39] Sahu, N. K. and S. K. Mishra, "Compact dual-band dual-polarized monopole antennas using via-free metasurfaces for off-body communications," *IEEE Antennas and Wireless Propagation Letters*, Vol. 21, No. 7, 1358–1362, 2022.

[40] Bait-Suwailam, M. M., I. I. Labiano, and A. Alomainy, "Impedance enhancement of textile grounded loop antenna using high-impedance surface (HIS) for healthcare applications," *Sensors*, Vol. 20, No. 14, 3809, 2020.

[41] Bait-Suwailam, M. M. and A. Alomainy, "Flexible analytical curve-based dual-band antenna for wireless body area networks," *Progress In Electromagnetics Research M*, Vol. 84, 73–84, 2019.